Pergamon

Geochimica et Cosmochimica Acta, Vol. 63, No. 19/20, pp. 3193–3203, 1999

0016-7037/99 $20.00 + .00

PII S0016-7037(99)00244-6

The role of Al in the formation of secondary Ni precipitates on pyrophyllite, gibbsite, talc, and amorphous silica: A DRS study

ANDREAS C. SCHEINOST,* ROBERT G. FORD, and DONALD L. SPARKS
Department of Plant and Soil Sciences, University of Delaware, Newark, Delaware 19717 USA

(*Received October* 15, 1998; *accepted in revised form April* 29, 1999)

Abstract—Formation of secondary Ni precipitates is an important mechanism of Ni retention in neutral and alkaline clay/water systems. However, the structure and composition of these secondary phases, and their stability is still disputable. Using existing structure refinement data and new ab-initio FEFF 7 calculations we show that Ni-edge X-ray absorption fine structure spectroscopy alone may not be able to unequivocally discriminate four possible candidate compounds: α-Ni(OH)$_2$, the isostructural but Al-substituted layered double hydroxide (Ni-Al LDH), and 1:1 and 2:1 Ni-containing phyllosilicates. Hence, we investigated the potential of diffuse reflectance spectroscopy (DRS) in determining in situ the Ni phase forming in the presence of four sorbents, pyrophyllite, talc, gibbsite, and amorphous silica. The $^3A_{2g} \rightarrow {}^3T_{1g}(F)$ band ($\nu 2$) of octahedrally coordinated Ni^{2+} could be reliably extracted from the reflectance spectra of wet pastes. In the presence of the Al-free talc and amorphous silica, the $\nu 2$ band was at $\approx$14,900 cm^{-1}, but shifted to 15,300 cm^{-1} in the presence of Al-containing pyrophyllite and gibbsite. This shift suggests that Al is dissolved from the sorbent and substitutes for Ni in brucite-like hydroxide layers of the newly forming precipitate phase, causing a decrease of the Ni-O distances and, in turn, an increase of the crystal-field splitting energy. Comparison with Ni model compounds showed that the band at 14,900 cm^{-1} is a unique fingerprint of α-Ni(OH)$_2$, and the band at 15,300 cm^{-1} of Ni-Al LDH. Although the complete transformation of α-Ni(OH)$_2$ into a Ni phyllosilicate causes a significant contraction of the Ni hydroxide sheet as indicated by band positions intermediate to those of α-Ni(OH)$_2$ and Ni-Al LDH, incipient states of silication do not influence Ni-O distances and cannot be detected by DRS. The first evidence for the formation of a precipitate was obtained after 5 min (pyrophyllite), 7 hr (talc), 24 hr (gibbsite), and 3 days (amorphous silica). For both pyrophyllite and talc, where sufficiently long time series were available, the $\nu 2$ energy slightly increased as long as the Ni uptake from solution continued (3 days for pyrophyllite, 30 days for talc). This may be explained by a relative decrease of relaxed surface sites due to the growth of crystallites. Our study shows that the formation of both α-Ni(OH)$_2$ and Ni-Al LDH may effectively decrease aqueous Ni concentrations in soils and sediments. However, Ni-Al LDH seems to be thermodynamically favored when Al is available.

1. INTRODUCTION

Recent studies have shown that the formation of secondary precipitates plays an important role in the retention of Ni and Co by clay minerals (Chisholm-Brause et al., 1989; Charlet and Manceau, 1994; O'Day et al., 1994a; 1996; Scheidegger et al., 1996a; 1998; Towle et al., 1997). Although the development of three-dimensional precipitates has been unequivocally proven by using X-ray absorption fine structure (XAFS) spectroscopy, their exact composition and structure has not been definitively determined. To match the observed Me–O and Me–Me distances, these researchers proposed either the formation of hydrotalcite-like layered double hydroxides (LDH; isomorphs of pyroaurite and green rust), 1:1 and 2:1 layer silicates, or the epitaxial growth of metal hydroxide monolayers at the surface of clay minerals with shorter bond distances compared to the free hydroxide. Another possible candidate not taken into account so far is the turbostratic, vacancy-rich variety of nickel hydroxide, α-Ni(OH)$_2$ (Bode et al., 1966; Pandya et al., 1990).

It is evident that a precise knowledge of the nature of these precipitates is crucial to predict the fate of Ni and Co in the environment, because the solubility of the precipitates strongly depends on their structure and composition. Scheidegger and Sparks (1996) found the precipitate that had formed in the presence of pyrophyllite more resistant to dissolution than β-Ni(OH)$_2$ at pH 4 and 6. Unpublished results from our group showed that the solubility of Ni reacted with pyrophyllite and talc decreased with increasing residence time, suggesting an alteration of the precipitate over time. Possible explanations for this alteration are (1) growth of larger crystals due to uptake of Ni from the solution or from smaller crystals by Ostwald ripening; (2) recrystallization to a more stable phase (e.g., α- to β-Ni(OH)$_2$); (3) changes in the elemental composition of a solid–solution (e.g., the Ni/Al ratio of LDH); or (4) transformation of LDH to a layer silicate by the attachment of SiO_2 polymers to the hydroxide layer, a process that has been observed in synthetic hydrothermal systems (Schutz and Biloen, 1987; Depège et al., 1996).

Determination of the structure of the precipitates is extremely difficult because of their low crystallinity and their dilution in a well-crystalline, Si- or Al-rich sorbent matrix. Thus, methods like X-ray diffraction (XRD), neutron diffraction, FTIR or NMR cannot be used for structural analysis. All of the candidate phases have a similar short-range order which makes their discrimination based on XAFS-derived Ni–O and

*Author to whom correspondence should be addressed (scheinos@udel.edu).

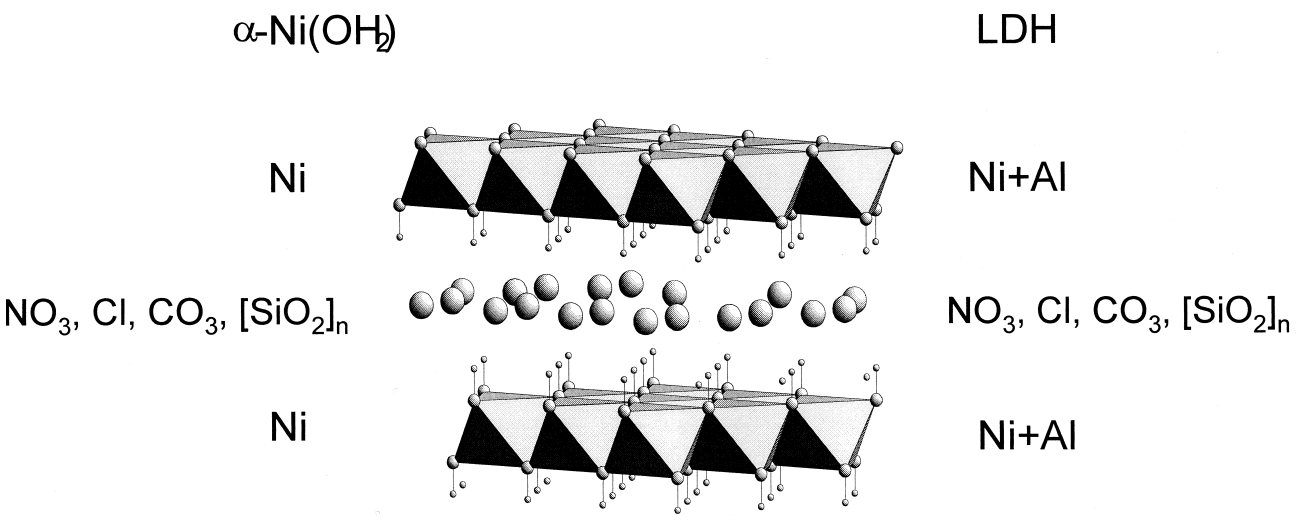

Fig. 1. Structure and composition of α-Ni(OH)$_2$ in comparison to layered Ni–Al double hydroxide (LDH). The R_{Ni-Ni} of α-Ni(OH)$_2$ is 3.07 Å (Pandya et al., 1990) and that of LDH is 3.05–3.08 Å (Bellotto et al., 1996). Both are turbostratic with a d-spacing of about 8 Å depending on the interlayer anions (Génin et al., 1991).

Ni–Ni distances impossible (see below). Therefore, other methods like TEM in combination with electron diffraction, XPS, and thermal methods have been used in addition to XAFS to elucidate the structure of similar precipitates (d'Espinose de la Caillerie et al., 1995; Burattin et al., 1997; Towle et al., 1997). It is evident that the reliability of the structure determination increases with the number of independent methods used; the intention of this study is to evaluate the potential of DRS in contributing to the characterization of the precipitates.

The crucial factor in the formation of Ni-Al LDH versus α-Ni(OH)$_2$ is the availability of Al. Results of d'Espinose de la Caillerie et al. (1995) and of Scheidegger et al. (1998) suggest a metal-promoted dissolution of the sorbents. However, in the study by Scheidegger et al. (1998) the concentration of Al in solution remained below detection limit ($<$50 ppb). To clarify whether Al is a prerequisite for the formation of a Ni-Al LDH secondary precipitate, we used pyrophyllite ($Al_2Si_4O_{10}(OH)_2$) and gibbsite (γ-Al(OH)$_3$) as Al-containing sorbents, and talc ($Mg_3Si_4O_{10}(OH)_2$) and amorphous silica (SiO_2) as Al-free sorbents. The sorption process was monitored over a period of four months to study aging effects. The precipitates forming at low Ni concentrations in the presence of sorbents were compared to model Ni compounds.

1.1. Limitations of XAFS in Identifying Ni Precipitates

The candidate phases for the secondary precipitates are composed of similar structural elements. Both α-Ni(OH)$_2$ and Ni-Al LDH consist of brucite-like layers (Fig. 1). The Al-for-Ni substitution in these layers creates a net positive charge that is balanced by hydrated anions in the interlayer space. In the case of the pure Ni hydroxide layers of α-Ni(OH)$_2$, the net positive charge is assumed to be created by hydroxyl vacancies (Génin et al., 1991) or by hydroxyl protonation (Kamath and Therese, 1997). Attaching SiO_2 polymers on one or both sides of the mono or double hydroxide layers generates 1:1 and 2:1 phyllosilicates.

Ni–O and Ni–Ni distances of the Ni candidate phases have been collected from the literature (Table 1). Missing Ni structures were substituted by the corresponding Mg compounds, justified by the similar ionic radii of Ni^{2+} (69 pm) and Mg^{2+} (72 pm) (Shannon, 1976). For comparison, the atomic distances of secondary Ni precipitates formed in the presence of pyrophyllite, gibbsite, and montmorillonite are shown in Table 1. The accuracy of XAFS-derived interatomic distances is $\pm$0.01 to 0.02 Å (Brown et al., 1988; O'Day et al., 1994b). Therefore, the Ni–O and Ni–Ni distances of the secondary precipitates coincide with those of α-Ni(OH)$_2$, Ni-Al LDH, nepouite, and pimelite, making the assignment to one phase arbitrary. Only the distances of β-Ni(OH)$_2$ and Ni carbonate are significantly different and therefore, can be excluded as possible candidates.

Discrimination of the other phases requires, however, the detection of Al atoms at a distance about the same as that of Ni or of Si neighbors at distances of 3.29 Å (1:1 phyllosilicate) or 3.24 Å (2:1 phyllosilicate) (Table 1). Ab-initio FEFF 7.0 calculations (Zabinsky et al., 1995) have been performed to investigate the influence of the weak backscatterers Si and Al on the Ni edge XAFS (Figs. 2 and 3). In accordance with the results of Manceau (1990), Al substituting for Ni dampens the second-shell amplitude, whereas Si at the larger distance of 3.24–3.29 Å enhances the second-shell amplitude. Consequently, fitted coordination numbers below the crystallographic value of 6 for the second shell may indicate the presence of Al, whereas a value above 6 may indicate Si. However, small clusters of nickel hydroxide with a high percentage of octahedra at edge positions and therefore, with less than six neighbors, or the presence of additional outer sphere sorbed Ni without neighbors, may reduce the statistical coordination number as well. Hence, neither bond distances nor coordination numbers of the first Ni–O shell and the first Ni–metal shell allow an unequivocal assignment to one of the possible phases. At higher radial distance, R, from the absorbing atom, a phase shift caused by Al or Si at the given distances from the central

Table 1. Atomic distances of Ni-reacted clay minerals (top) in comparison with those of matching (middle) and non-matching Ni compounds (bottom).

Sample	R_{Ni-O}/Å	CN	R_{Ni-Ni}/Å	CN	R_{Ni-Al}/Å	CN	R_{Ni-Si}/Å	CN	Method	Source
Pyrophyllite (1 d)	2.05	(5.5)	3.05	(4.9)	3.08	(1.7)			XAFS	(Scheidegger et al., 1998)
Gibbsite (28 d)	2.04	(5.8)	3.06	(6.6)	3.10	(3.1)			XAFS	(Scheidegger et al., 1998)
Montmorillonite (38 d)	2.04	(6.1)	3.07	(6.5)	3.11	(1.0)			XAFS	(Scheidegger et al., 1998)
Hydrotalcite (Mg/Al = 2)	2.01	(6.0)	3.05	(3.0)	3.05	(3.0)			XRD	(Bellotto et al., 1996)
Hydrotalcite (MG/Al = 5)	2.04	(6.0)	3.08	(5.0)	3.08	(1.0)				
Talc/Pimelite	2.06	(6.0)	3.06	(6.0)			3.24	(4.0)	XRD	(Perdikatsis and Burzlaff, 1981)
Ni/Al LDH	2.05	(6.5)	3.06	(4.8)	3.06	(1.4)			XAFS	(d'Espinose de la Caillerie et al., 1995)
α-$Ni(OH)_2$	2.04	(5.8)	3.07	(5.7)					XAFS	(Pandya et al., 1990)
Lizardite/ Nepouite	2.06	(6.0)	3.08	(6.0)			3.29	(2.0)	XRD	(Mellini, 1982)
β-$Ni(OH)_2$	2.07	(6.0)	3.13	(6.0)					XRD	(Greaves and Thomas, 1986)
$NiCO_3$	2.08	(6.0)	3.62	(6.0)					XRD	(Pertlik, 1985)

Coordination numbers are given in parentheses.

Ni should be detectable. In practice, however, the low overall signal resulting from relatively low concentrations of Ni in the reacted clay samples, the decrease of the signal-to-noise ratio with increasing R, and the accumulation of multiple scattering paths at higher R may prevent a proper assignment (Manceau and Decarreau, 1988).

1.2. Potential of DRS in Identifying Ni Precipitates

Electronic spectroscopy has a long tradition in determining oxidation state and coordination of transition metals in minerals and synthetic compounds, using both transmission and diffuse reflectance techniques (Orgel, 1952; Lever, 1984; Burns, 1993). Due to its ability to probe low concentrations of cations with short-range order only and in situ, recently DRS has been used to study Ni and other transition metals in catalysts (Schoonheydt et al., 1987; Weckhuysen et al., 1994; Kermarec et al., 1995; Verberckmoes et al., 1995; Davidson et al., 1996). The bands detected by this technique are caused by the splitting of the energy levels within the incompletely-filled shell of 3d electrons through symmetry-dependent interaction with the negative charge of the surrounding ligands. For Ni^{2+} ($3d^8$) in octahedral coordination, three spin-allowed transitions are predicted to arise from the ground level $^3A_{2g}$ in the UV-VIS-NIR spectral range covered by our investigation (Fig. 4) (Liehr and Ballhausen, 1959). The lowest energy transition, $^3A_{2g}(^3F) \rightarrow {}^3T_{2g}(^3F)$ (band $\nu 1$), is a linear function of only the crystal-field splitting energy Dq, whereas the other two transitions, $^3A_{2g}(^3F) \rightarrow {}^3T_{1g}(^3F)$ (band $\nu 2$) and $^3A_{2g}(^3F) \rightarrow {}^3T_{1g}(^3P)$ (band $\nu 3$), are functions of Dq and Racah-B (Lever, 1984; Burns, 1993). A spin-forbidden triplet-singlet transition, $^3A_{2g}(^3F) \rightarrow {}^1E_g(^1D)$ (band sf), may be enhanced by spin-magnetic coupling with $\nu 2$ when close enough to this spin-allowed band (Reinen, 1966).

From crystal-field theory, a fifth-power relationship between the metal–ligand bond distance and Dq could be derived (Lever, 1984), which recently has been confirmed by ab-initio molecular-orbital calculations (Krasovska et al., 1997). Thus, band energies of $\nu 1$, $\nu 2$, and $\nu 3$ should be shifted by even small changes in metal–ligand distances. The second factor influencing the band energies of $\nu 2$ and $\nu 3$, Racah-B, varies with the covalence of the metal–ligand bond (Lever, 1984). Although the covalence is mainly determined by the electronic properties of a given metal–ligand pair, a reduction of the metal–ligand distance by inducing pressure did not only change Dq, but also Racah-B (Abu-Eid and Burns, 1976).

Using polarized transmission spectroscopy for determining the 3d band positions, Faye (1974) found a positive relationship between R_{Ni-O} of several Ni minerals and band positions, and Reinen (1969) observed band shifts for a solid–solution containing the larger Cr^{3+} versus the smaller Al^{3+}. Using a refined method to extract the band positions from DRS spectra, Scheinost et al. (1999) showed a similar trend for Al substitution in goethite. Because of its higher sensitivity to changes of first-shell bond distances, DRS favorably complements short-range order determinations by XAFS (Marco de Lucas et al., 1995). Therefore, we expect the spin-allowed bands of Ni^{2+} to shift toward higher energies when Al substitutes for Ni in hydroxide layers and decreases R_{Ni-O}.

2. MATERIALS AND METHODS

The N_2-BET surface areas of the sorbent phases used in this study are 95 $m^2\ g^{-1}$ for pyrophyllite, 75 $m^2\ g^{-1}$ for talc, 25 $m^2\ g^{-1}$ for gibbsite, and 90 $m^2\ g^{-1}$ for the amorphous silica (Zeofree 5112, Huber Company). The mean particle size of the amorphous silica is 10 μm (Microtrac method), particle size of the other sorbents is <2 μm (Stokes diameter). XRD showed minor impurities of kaolinite and quartz in pyrophyllite, about 10% bayerite in the gibbsite, and about 20% chlorite in talc, whereas the amorphous silica was pure. After acid digestion, an Al/Mg ratio of 0.01 was found for the talc sample, confirming its low Al content. Therefore, even with these impurities, the classification of the sorbents as Al-rich (pyrophyllite, gibbsite) and Al-poor (talc, silica) phases is valid. Preparation of the samples was as described in Scheidegger et al. (1996b; 1998). Ni model compounds

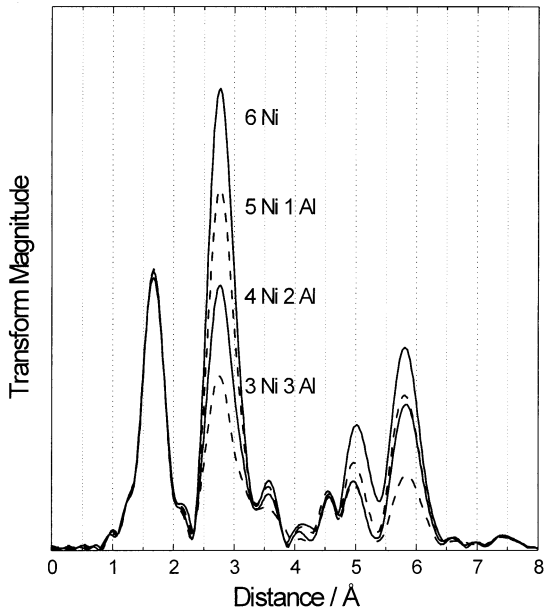

Fig. 2. Full multiple-scattering FEFF simulations showing the dampening of the Ni–Ni amplitude by increasing Al-for-Ni substitution (given as number of atoms in the first metal shell). The clusters are based on the structure of Mg:Al = 5 hydrotalcite (Bellotto et al., 1996). The endmember with 6 Ni is analogous to α-Ni(OH)$_2$ based on R_{Ni-O} and R_{Ni-Ni} given by Pandya et al. (1990).

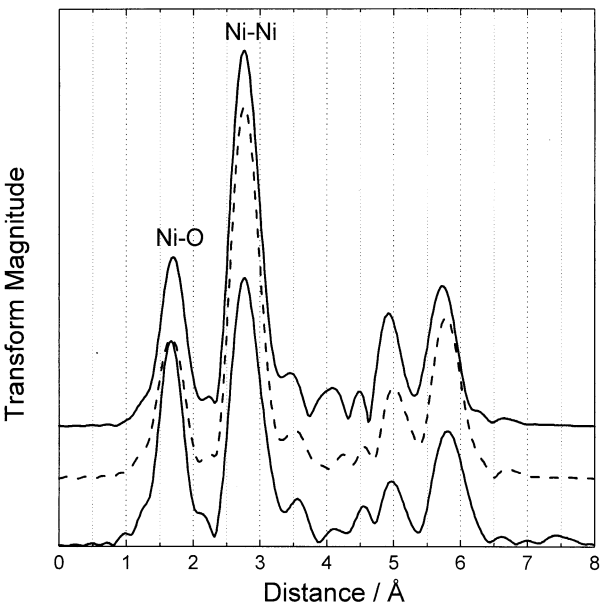

Fig. 3. Full multiple-scattering FEFF simulations of clusters of pimelite, nepouite, and Ni–Al LDH (from top to bottom), derived from the structures of talc (Perdikatsis and Burzlaff, 1981), lizardite (Mellini, 1982) and hydrotalcite (Bellotto et al., 1996), respectively.

were synthesized as described in Table 2, and identified by XRD and FTIR (A. C. Scheinost and R. G. Ford, unpublished).

Experiments were run at pH 7.5 and 22°C in a background electrolyte of 0.1 M $NaNO_3$. An initial Ni concentration of 1.5 mM and a solids concentration of 5 g/L was used. These experimental conditions, including the initial solids surface area to total Ni concentration, are consistent with conditions used by Scheidegger et al. (1997; 1998). Experimental systems were either saturated (Ω = 1.08) or undersaturated with respect to β-Ni(OH)$_2$ based on reported solubility constants which range from logK = −10.8 to logK = −18 (Mattigod et al., 1997).

The sorbents were hydrated in the background electrolyte for 24 hr on a reciprocal shaker. The suspensions were then transferred to a pH stat apparatus, and vigorously stirred with a magnetic stir bar and purged with N_2 to eliminate CO_2. The pH was adjusted to 7.5 using 0.1 M NaOH. After equilibration for 2 hr, an appropriate amount of Ni from a 0.1 M Ni$(NO_3)_2$ stock suspension was added in three steps within a 2 min period to achieve the initial Ni concentration of 1.5 mM. The pH was controlled for 2–4 days by using the pH stat apparatus (±0.05 units) followed by manual adjustments (±0.2 units) for the subsequent aging periods. After the desired reaction periods, aliquots of the suspension were collected and immediately centrifuged at 14,000 rpm and 2°C for 5 min. The supernatant was passed through a 0.22 μm membrane filter and analyzed for Ni, Si, Al, and Mg by ICP. The amount of Ni sorbed was calculated from the difference between the initial and the final Ni concentrations. The remaining wet pastes were washed once with 0.1 M $NaNO_3$ to remove excess Ni in the entrained electrolyte, and centrifuged again. The samples were analyzed by DRS immediately after sampling.

Diffuse reflectance spectra were measured with a double-beam Lambda 9 spectrophotometer equipped with a Spectralon-coated integrating sphere 5 cm in diameter (Perkin Elmer). The wavelength was internally calibrated against the emission lines of deuterium. Spectra were recorded from 1600 to 300 nm in 1 nm steps, with a scan speed of 60 nm/min, a response time of 2 s, and a NIR gain of 2. Collection time for each spectrum was 30 min. In the visible range, a constant slit width of 2 nm was used for the monochromator, and the reflected radiation was detected with a photon multiplier detector. In the NIR range, the slit width was automatically increased with decreasing wave number to maintain a sufficient energy throughput to the PbS detector. The wet pastes were filled in an aluminum holder 10 mm in diameter and 1 mm in depth protected by parafilm. The pastes were covered with a microscope cover slide to allow measurement of the sample in a vertical orientation. To account for absorption by the glass slide, the reflectance was calibrated against a Spectralon standard (Labsphere) covered with another slide. Possible aging effects for samples collected

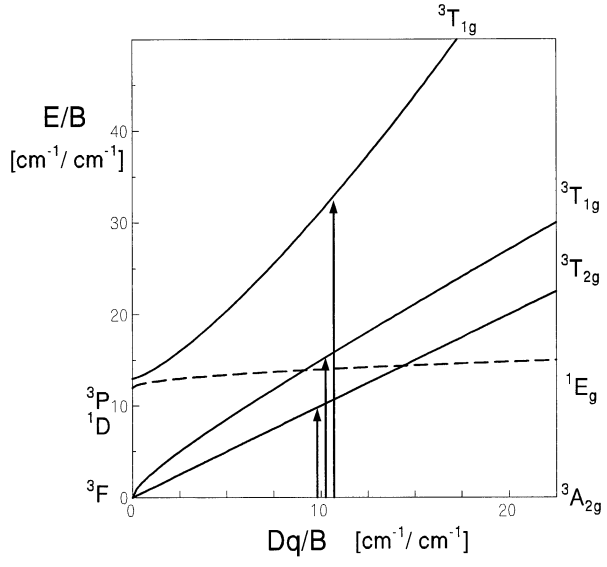

Fig. 4. Crystal-field splitting of Ni^{2+} in octahedral coordination. Energy levels, *E*, are given as functions of the crystal-field splitting energy, *Dq*, and the Racah parameter *B*. Units of both axes are cm^{-1}/cm^{-1}.

Table 2. Al-substitution (x_{Al} in mole fraction) and $\nu 2$ band position [$cm^{-1} * 10^{-3}$] of Ni reference compounds used in this study.

Sample Name	Sample Description and Preparation	X_{Al}	$\nu 2$
LDH 2:1	Ni-Al LDH with NO_3 interlayer by coprecipitation at pH 7.5, initial Ni:Al ratio of 2 (Taylor, 1984)	0.43	15.30
LDH 4:1	as above, but initial Ni:Al ratio of 4	0.30	15.31
LDH 10:1	as above, but initial Ni:Al ratio of 10	0.31	15.37
LDH 10:1 cop	Ni-Al LDH with NO_3 interlayer by coprecipitation method, initial Ni:Al ratio of 10 (Depège et al., 1996)	0.20	15.41
LDH SiO_2 exchanged	Ni-Al LDH with SiO_2 interlayer by exchange of NO_3 with SiO_2 at pH 7.5 (Depège et al., 1996)	0.29	15.34
LDH SiO_2 coprecip.	Ni-Al LDH with SiO_2 interlayer by coprecipitation with SiO_2 at pH 7.5, initial ratio of Ni:Si:Al = 3:1:1 (Depège et al., 1996)	0.20	15.26
LDH SiO_2 hydrothermal	as above, but aged at 150°C for 2 wk	nd[a]	15.23
Ni silicate ini	Ni silicate, fresh precipitate (Grauby et al., 1993)	0	14.90
Ni silicate 2 wk	as above, hydrothermally aged at 150 °C for 15 d (Grauby et al., 1993)	0	15.16
Nepouite	natural nepouite from Riddle, Oregon	nd[a]	15.15
Garnierite	natural garnierite from Victorio, New Mexico	nd[a]	15.16
α-$Ni(OH)_2$ ini	α-$Ni(OH)_2$, initial precipitate (Gènin et al., 1991)	0	14.90
α-$Ni(OH)_2$ aged	α-$Ni(OH_2)$, as before, but aged for 4 days at RT (Génin et al., 1991)	0	14.75
NiSiMg coprecip.	α-$Ni(OH)_2$ by coprecipitation of $Ni(NO_3)_2$, Na_2SiO_3 and $Mg(NO_3)_2$ at pH 8.5, initial ratio of Ni:Si:Mg=4:2:1	0	14.88
$NiCO_3$	crystalline $NiCO_3$, Johnson & Matthey	0	14.65
Aqueous $Ni(NO_3)_2$	0.1 *M* $Ni(NO_3)_2$ Johnson & Matthey	0	14.43

[a] Not determined.
Except for the natural minerals and the commercially available chemicals, these solids were synthesized using the methods given in column 2.

at reaction times shorter than 12 hr were avoided by initially scanning through the 900 to 500 nm range (10 min). As shown later, this spectral range brackets the $\nu 2$ band most important for analysis. After this step, a scan across the full spectral range was collected.

3. RESULTS AND DISCUSSION

3.1. Kinetics of Ni Removal

As shown in Fig. 5, 95% of Ni was removed from solution within 3 days by pyrophyllite and within 4 wk by talc. In the presence of gibbsite, 50% of Ni was removed within 4 months. Although data on amorphous silica were collected only for 26 days, a trend similar to that of gibbsite is evident. The much faster reaction with pyrophyllite than with gibbsite is consistent with results shown by Scheidegger et al. (1998). In that study, however, pyrophyllite removed 95% of Ni in <1 day, and gibbsite removed 90% within 24 days. The slower reaction kinetics in our study may be explained by the lower Ni concentration (1.5 mM instead of 3 mM) reducing the (unknown) degree of supersaturation with respect to the forming precipitates (explained below). The presence or absence of Al in the sorbents does not seem to be a major factor controlling the kinetics of precipitation, because the reaction kinetics of both the pyrophyllite and talc systems are similar and much higher than those of the gibbsite and silica systems.

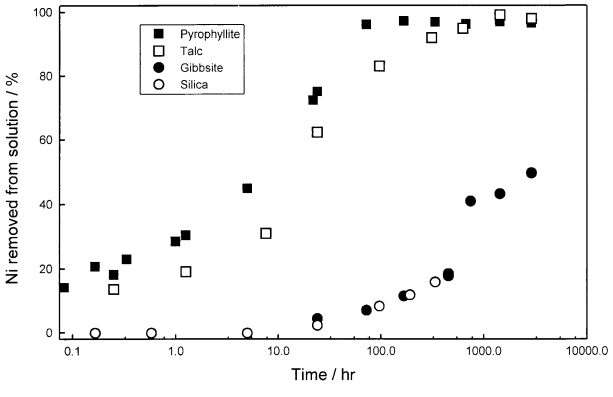

Fig. 5. Ni removal from solution as a function of time in the presence of pyrophyllite, talc, gibbsite, and amorphous silica.

As in the study by Scheidegger et al. (1998), the Al concentration in solution was below the detection limit. Si (pyrophyllite, talc, and amorphous silica) and Mg (talc), however, were released during reaction with Ni (Fig. 6), indicating sorbent dissolution. In the case of pyrophyllite, the Si release was almost log-linear over four months and did not decrease when the Ni concentration reached a steady state after 3 days. This may indicate that at least the long-term dissolution of pyrophyllite was not enhanced by Ni, in contrast to the Ni-promoted dissolution suggested by earlier work (d'Espinose de la Caillerie et al., 1995; Scheidegger et al., 1998).

3.2. Identification of Secondary Precipitates by DRS

The raw diffuse reflectance spectrum of hydrated, unreacted pyrophyllite (Fig. 7, top spectrum) shows OH overtone and combination bands resulting from structural hydroxyls and water at about 6900 cm^{-1} (partly cut-off), and free water at 8450, 10,250, and 11,500 cm^{-1}. Starting at about 20,000 cm^{-1}, reflectance decreases with increasing wave number. Although the long-range decline can be explained by a broad O–Al charge transfer band with a maximum in the UV, the much narrower band at about 26,500 cm^{-1} is indicative of Fe^{2+} impurities in pyrophyllite. The spectra of hydrated talc and gibbsite are similar to that of pyrophyllite. The spectrum of amorphous silica extends featureless into the UV where a steep

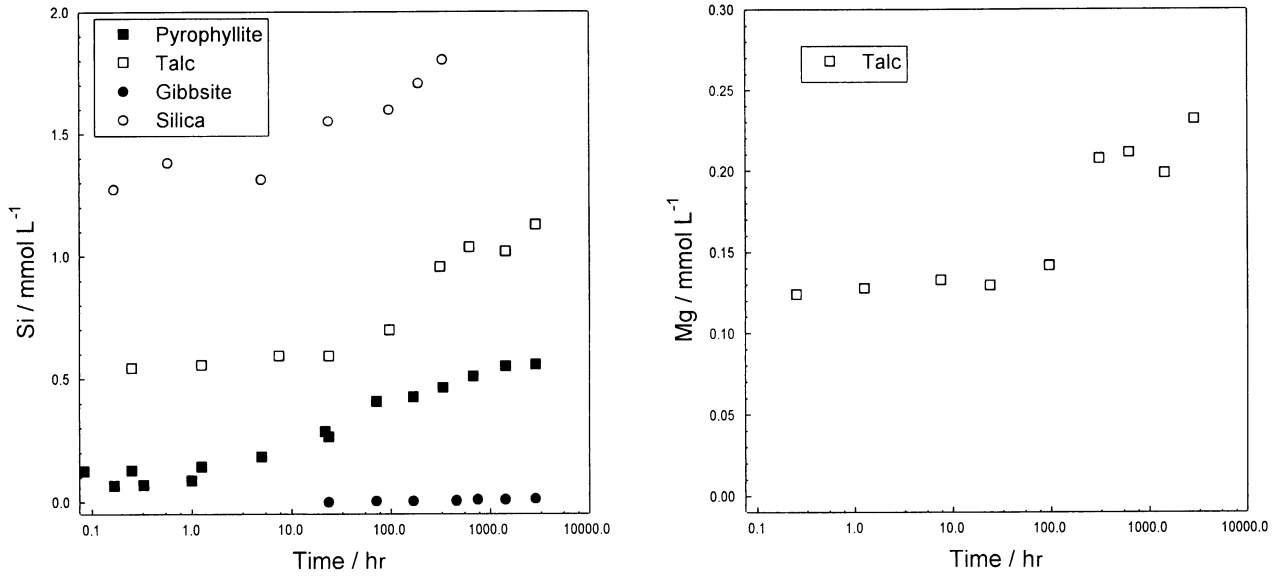

Fig. 6. Rate of Si and Mg release from pyrophyllite, talc, gibbsite, and amorphous silica.

slope at about 28,000 cm^{-1} resulting from the O–Si charge transfer develops (not shown).

With increasing duration of the Ni treatment, a double band at about 15,000 cm^{-1} develops in addition to the features described above (Fig. 7). Making a ratio of the spectra against that of the untreated sample, and converting the resulting reflectance spectra into absorbance by using the Kubelka–Munk equation (Kubelka and Munk, 1931) revealed three bands at about 9200, 15,400, and 25,800 cm^{-1} with the intensity increasing with Ni uptake (Fig. 8). These bands arise from the three spin-allowed crystal-field bands of Ni^{2+} in sixfold coordination: $^3A_{2g}(^3F) \rightarrow {}^3T_{2g}(^3F)$ (band $\nu1$), $^3A_{2g}(^3F) \rightarrow {}^3T_{1g}(^3F)$ (band $\nu2$), $^3A_{2g}(^3F)$ ($\rightarrow {}^3T_{1g}(^3P)$ (band $\nu3$) (see Fig. 4). The shoulder at the low-energy side of $\nu2$ at about 13,800 cm^{-1} is the spin-forbidden transition $^3A_{2g}(^3F) \rightarrow {}^1E_g(^1D)$ (band sf). In comparison with spectra of Ni minerals (Manceau et al., 1985), the shape of $\nu1$ of all samples is strongly distorted and cut off at the low-energy side. This seems to be an artifact resulting from the background removal in a spectral range which is dominated by much stronger vibrational bands (Fig. 7). Applying the same background removal procedure to spectra of freeze-dried samples indeed recovered the expected symmetrical $\nu1$ band (not shown). Furthermore, $\nu3$ could not be determined reliably for the wet talc samples. Thus, only $\nu2$ remained for the in situ investigation of the secondary precipitates in all systems. Its position was determined by deconvolution with Gaussian line shapes.

To test how reliably the position of $\nu2$ could be determined, we prepared physical mixtures of Ni-Al LDH and α-$Ni(OH)_2$ with unreacted pyrophyllite and talc, and measured these mixtures as both dry powders and wet pastes (not shown). We applied the same spectral treatment (background removal) as for the spectra of Ni-reacted samples. The $\nu2$ positions determined by this method always corresponded to those of the

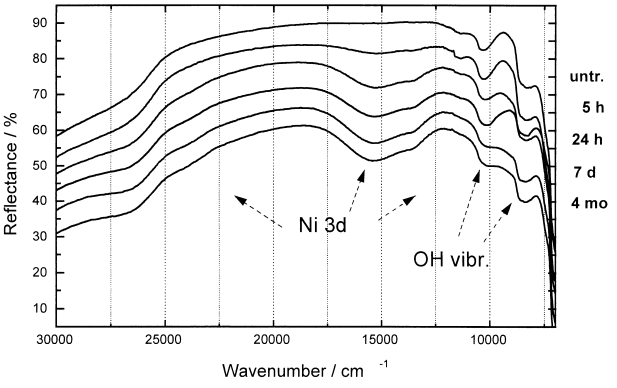

Fig. 7. Time-resolved diffuse reflectance spectra for wet pastes of Ni-reacted pyrophyllite.

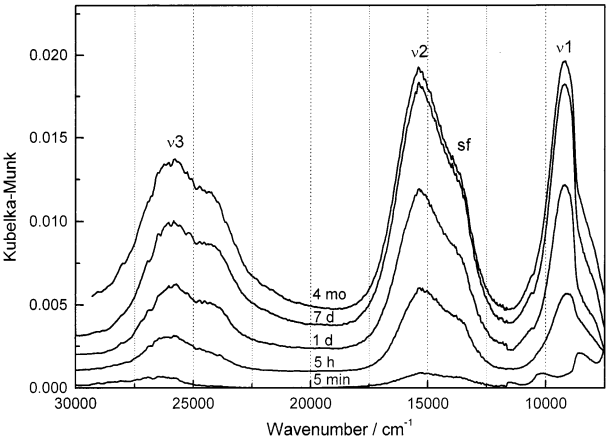

Fig. 8. Absorption bands of Ni^{2+} in Ni-reacted pyrophyllite. The bands have been extracted by making a ratio of the diffuse reflectance spectra for the Ni-reacted samples with that of the untreated, hydrated sample, then transformed into absorption spectra by using the Kubelka–Munk equation. See text for the band assignment.

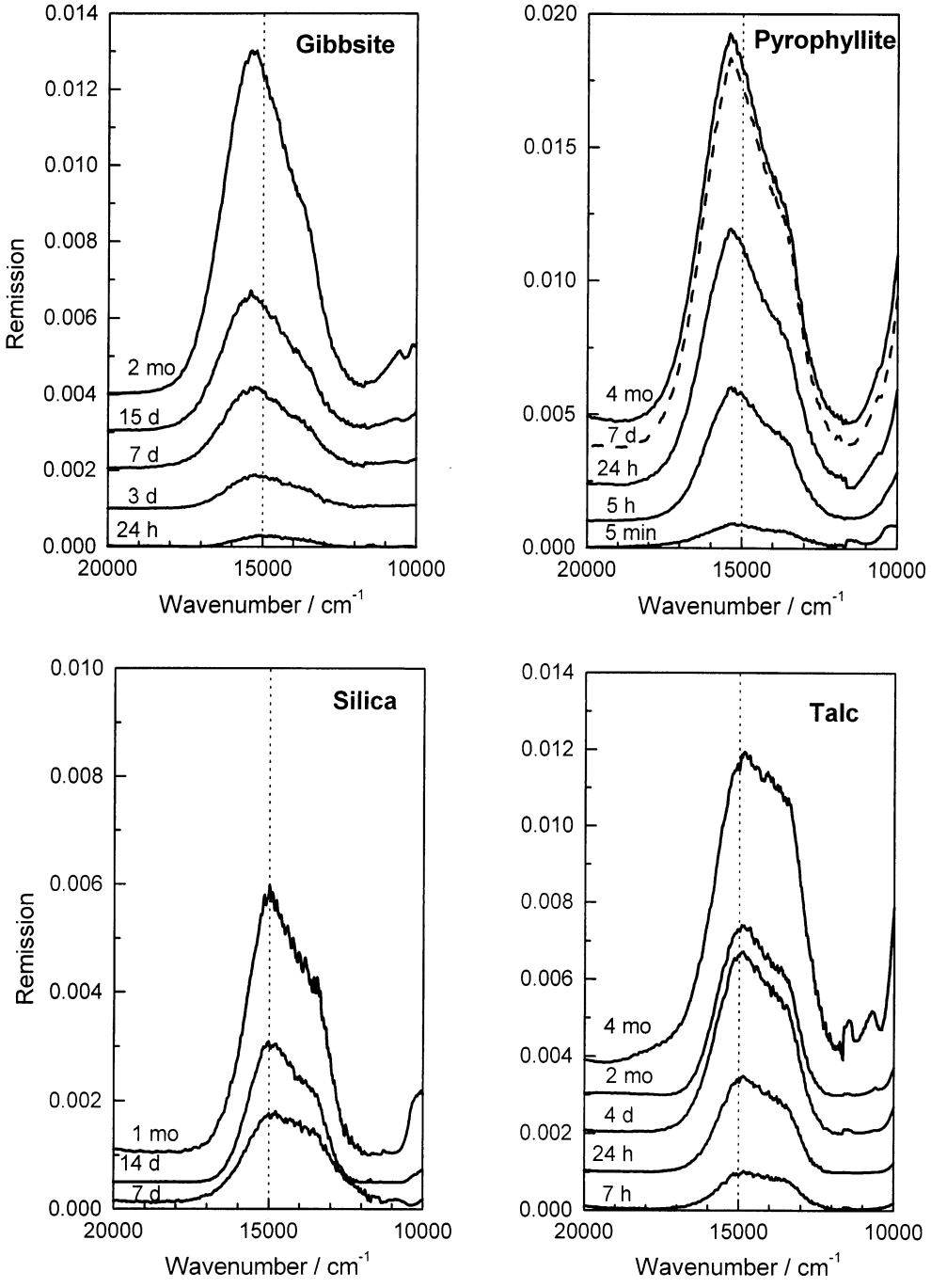

Fig. 9. The time-resolved $\nu 2$ bands of the Ni precipitate in presence of the two Al-containing sorbents gibbsite and pyrophyllite (top) versus those in the presence of the Al-free sorbents talc and amorphous silica (bottom).

respective pure reference compounds and showed the clear separation between Ni-Al LDH and α-$Ni(OH)_2$. No significant influence of Ni concentration, type of clay mineral, or moisture content could be found. The variation of the $\nu 2$ energy of a given Ni compound was always within ± 30 cm^{-1} of the average and therefore, much lower than the differences between the model compounds (Table 2).

The intensity of $\nu 2$ increased for all four sorbents with increasing reaction time (Figs. 9 and 10). The peak positions in presence of the two Al-containing minerals, gibbsite and pyrophyllite, are at about 15,300 cm^{-1}, whereas those of silica and talc are at about 14,900 cm^{-1}. In Fig. 11, the fitted band positions are plotted as a function of time, and shown together with hatched areas representing the range of $\nu 2$ position of synthetic Ni model compounds (Table 2). The two different band positions are well separated throughout the reaction period. The higher wave number of Ni-reacted pyrophyllite and gibbsite suggests the formation of a precipitate with Ni in a

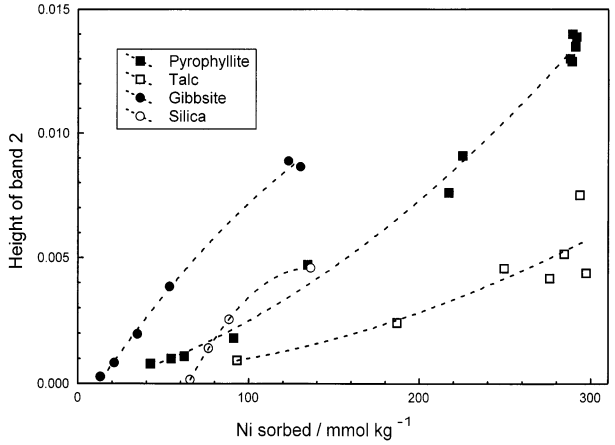

Fig. 10. Height of $\nu 2$ versus quantity of Ni precipitates calculated from [Ni] in solution.

brucite-like hydroxide layer partly substituted by Al. In contrast, precipitates formed in systems containing talc and silica appear more consistent with pure α-Ni(OH)$_2$. The $\nu 2$ of $NiCO_3$ would be at a significantly lower wave number than that of the secondary precipitates (Table 2). Minor quantities of aqueous Ni^{2+} may be adsorbed to pyrophyllite and talc as an outer sphere complex. Due to the weak crystal field caused by six water molecules surrounding Ni^{2+}, the absorption coefficient of aqueous Ni^{2+} is much smaller than that of the solid Ni phases. Therefore, these small amounts of sorbed Ni^{2+} may not be detectable by DRS, although the $\nu 2$ would occur at an energy well below that of the solid phases (Table 2).

The data shown so far confirm that Al-substitution decreases R_{Ni-O} because of a smaller radius for Al^{3+} compared to Ni^{2+}, as has been shown for other ion pairs with similar radius ratios (Orgel, 1957). The magnitude of the shift is comparable to that of Cr^{3+} in corundum (Reinen, 1969) and Fe^{3+} in Al-substituted goethite (Scheinost et al., 1999) for an Al mole fraction of 0.33. These investigators found a quasi-linear relationship between Dq and the Al substitution. The $\nu 2$ of the Ni-Al LDH samples, however, did not show the expected positive correlation with Al substitution ranging from 0.20 to 0.43 mole fraction (Table 2). This may be an effect of mixing of the spin-allowed transition $^3A_{2g}(^3F) \rightarrow {}^3T_{1g}(^3F)$ with the spin-forbidden transition $^3A_{2g}(^3F) \rightarrow {}^1E_g(^1D)$, which is largely independent of Dq (Fig. 4). Consequently, the Al-substitution cannot be estimated from $\nu 2$.

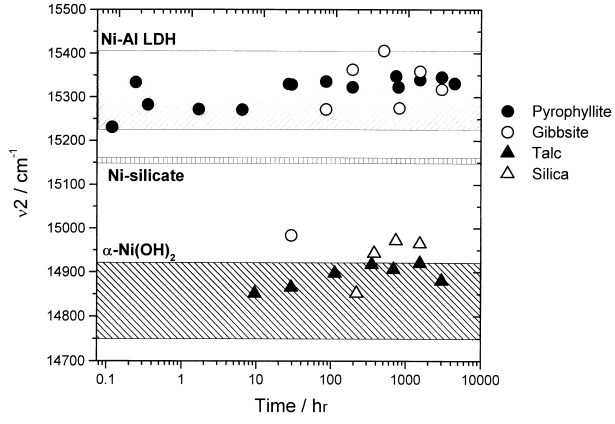

Fig. 11. Fitted $\nu 2$ band positions of the Ni reacted minerals (dots and triangles) over time. The range of the $\nu 2$ band positions of Ni reference compounds (Table 2) is given by the hatched areas.

Trioctahedral Ni phyllosilicates consist of the same brucite-like sheet as α-Ni(OH)$_2$ and Ni-Al-LDH with silicate sheets attached on one or both sides. The neoformation of phyllosilicates is one way to explain earlier XAFS data of Ni and Co reacted with clay minerals (Charlet and Manceau, 1994). The formation of these phyllosilicates may proceed either by heterocondensation of aqueous Ni and Si species (Burattin et al., 1995; 1997), or by addition of silica to hydrotalcite-like precursors (Depège et al., 1996). In our study, substantial Si concentrations built up over time in the presence of pyrophyllite, talc, and silica (Fig. 6), which could have initiated the formation of Ni phyllosilicates. However, crystalline Ni phyllosilicates would be clearly distinguishable from α-Ni(OH)$_2$ and Ni-Al LDH, because of intermediate $\nu 2$ band positions that are inconsistent with the $\nu 2$ of the surface precipitates (Table 2 and Fig. 11). This intermediate position may be explained by the contraction of the Ni hydroxide sheets in phyllosilicates compared to bare hydroxide layers, caused by a size mismatch between the hydroxide and the silicate sheets (Charlet and Manceau, 1994). However, the $\nu 2$ of a fresh Ni silicate precipitate was identical to the $\nu 2$ of α-Ni(OH)$_2$ and silicate exchanged LDH samples had $\nu 2$ positions comparable to those of Ni-Al LDH (Table 2). This implies that early stages of phyllosilicate formation, where only small clusters of silicate may be attached to the Ni hydroxide layers, cannot be distinguished from the Si-free hydroxides by using DRS. Indeed, high-resolution thermogravimetric analyses showed that such Ni–Al phyllosilicate precursors formed in the presence of pyrophyllite within 1 year (Ford et al., 1999).

3.3. Aging of Secondary Precipitates

The first signal from Ni-Al LDH clusters was measured after 5 min in the pyrophyllite system, and after 24 hr in the gibbsite system (Figs. 9 and 11). Thus, we could detect the formation of precipitates with DRS at earlier stages than Scheidegger et al. (1998) with XAFS, although the rates were even slower in the present study. For talc, the first signal was observed after 7 hr. A detectable precipitation of α-Ni(OH)$_2$ in the presence of amorphous silica was not observed until after 3 days. The band height of $\nu 2$ showed a close correlation to the amount of precipitate formed in the systems (Fig. 10). Every system had, however, a different slope. This may be explained by several reasons, including (1) differences in the absorption coefficients of the two structurally different precipitates; (2) differences in the precipitate-to-clay surface ratio; (3) differences in particle size of precipitates and clay minerals; (4) differing light scattering properties of the clay minerals; or (5) a low correlation between Ni removed from solution and the amount of precipitate formed in response to variable ratios between adsorbed and precipitated Ni. Because of these uncertainties, no further

attempt was made to establish a quantitative relationship between the mass of precipitates and peak intensities. Depending on the sorbent phase, the lower detection limit for the precipitates varied between 10 and 30 mmol kg^{-1} (600–1800 ppm; Fig. 10).

During the initial phase of nucleation and crystal growth until Ni uptake from solution reaches 95% (i.e., at about 100 hr in the pyrophyllite system; Fig. 5), $\nu 2$ significantly increased in wave number, but stayed constant beyond that point (Fig. 11). A similar tendency, an increase of $\nu 2$ up to about 700 hr, then scattering around a maximum value, can be observed in the presence of talc. In both cases, the increase in wave number indicates a contraction of R_{Ni-O}. The contraction over time may be explained by initially small clusters with a high percentage of edge positions, and a large contribution of relaxed R_{Ni-O} to the average bond distance. Growth of larger crystallites with time would decrease the relative contribution of the relaxed surface sites and thus decrease R_{Ni-O}. As a result of insensitivity of $\nu 2$ to variations of the Al substitution of the model compounds, decrease of R_{Ni-O} corresponding with increasing Al substitution is an unlikely explanation for the band shift. In the presence of gibbsite, the first detectable precipitate formed after 1 day (Figs. 9 and 11). Despite a high standard deviation in $\nu 2$ of 60 cm^{-1} resulting from low peak intensity, the band energy of this sample is significantly below that of precipitates at later time steps. This suggests an initial formation of α-$Ni(OH)_2$ or a mixture of α-$Ni(OH)_2$ and Ni-Al LDH, whereas at later times only LDH forms.

3.4. Mechanisms of Precipitate Formation

The preferential formation of Ni-Al LDH in the presence of the Al-containing minerals, pyrophyllite and gibbsite, indicates both the dissolution of the sorbent phase, and either a higher thermodynamic stability or a faster precipitation of Ni-Al LDH than α-$Ni(OH)_2$. Consequently, the formation of α-$Ni(OH)_2$ in the presence of gibbsite within the first 24 hr can be explained by a slower rate of Al release compared to pyrophyllite. This may be caused by the higher stability of gibbsite in contrast to that of pyrophyllite as long as the concentration of silicic acid exceeds $10^{-4.3}$ M (Lindsay, 1979; Hemingway and Sposito, 1996), a condition always fulfilled in the pyrophyllite system (Fig. 6). After three days, about twice as much Ni is taken up by the precipitate phase, which is now solely Ni-Al LDH. Therefore, the initial α-$Ni(OH)_2$ phase transformed into Ni-Al LDH. This phase transformation strongly supports the hypothesis that the preferential formation of Ni-Al LDH is the result of a higher thermodynamic stability rather than of faster reaction rates.

The polymerization reaction leading to Ni-Al LDH may proceed via Ni–OH–Ni, Al–OH–Al, and Ni–OH–Al olation reactions similar to those proposed by Burattin et al. (1995; 1998). Of greater interest is the question of how Al is provided by the sorbent phase. Scheidegger et al. found evidence for a Ni-promoted dissolution of pyrophyllite (d'Espinose de la Caillerie et al., 1995; Scheidegger et al., 1998). In our study, [Si] increased even after [Ni] had reached a steady state, indicating that pyrophyllite dissolution continued. [Si] was $\geq$0.1 mM. Assuming a congruent dissolution of pyrophyllite, [Al] $\geq$0.05 mM would result, in contrast to our observation that [Al] was below the 0.002 mM detection limit. This much lower value may indicate a rapid uptake by the growing Ni-Al LDH phase. An alternative explanation would be the intermediate formation of an Al hydroxide phase. At pH 7.5, the solution is supersaturated with respect to diaspore for [Al] $\geq 10^{-5}$ mmol/L of [Al] (Hemingway and Sposito, 1996). Depending on the (unknown) stability of Ni-Al LDH, and following the Ostwald step rule, two scenarios can be proposed: (1) If Ni-Al LDH is less stable than diaspore, it would act as the immediate sink for Al; and (2) If Ni-Al LDH is more stable, diaspore would form first, but subsequently transform into Ni-Al LDH, possibly involving other intermediate Al hydroxide phases. Because of the fast formation of Ni-Al LDH ($<$5 min) we favor immediate transfer of Al from pyrophyllite to LDH. Diaspore may form, however, after about three days, when the Ni depletion from solution reaches a steady state, but pyrophyllite still dissolves as indicated by a continued release of Si (Fig. 6). This Si may eventually cause the transformation of the Ni-Al LDH phase into a Ni–Al phyllosilicate precursor (Ford et al., 1999), a process apparently not detected by DRS.

In the presence of the Al-free sorbents talc and silica, α-$Ni(OH)_2$ formed. As a result of the distinguishable $\nu 2$ positions of α-$Ni(OH)_2$ and Ni phyllosilicate, the formation of a crystalline phyllosilicate within the first months can be excluded. However, a Ni phyllosilicate precursor may have formed, consisting of α-$Ni(OH)_2$ with silicate polymers in the interlayer. A Ni–O–Si heterocondensation as proposed by Burattin et al. (1995; 1998) seems to be less likely, because it should result in contracted Ni hydroxide sheets from the beginning. Different reaction paths in our study may be explained by the two orders of magnitude higher initial [Ni] and the one order of magnitude lower proton concentration compared to the study by Burattin et al. (1995; 1998).

Although the formation of α-$Ni(OH)_2$ in the presence of talc is slower than the formation of Ni-Al LDH in the presence of pyrophyllite, the differences between the talc and silicate systems, or between the pyrophyllite and gibbsite systems are greater. Therefore, factors other than the availability of Al have a larger influence on the rates of Ni precipitation. These factors may include the sorbent surface area and selectivity for Ni, which could enhance local [Ni] at the mineral–water interface. Thus, although the formation of both precipitate phases can reduce [Ni] far below the level achieved by adsorption, the time to reach equilibrium varies greatly depending on the sorbent phase. In the presence of pyrophyllite–montmorillonite mixtures, precipitation of Ni-Al LDH and adsorption of Ni onto montmorillonite were both equally fast processes for Ni removal (Elzinga and Sparks, 1999). Over longer time scales, however, formation of a precipitate may solely control the availability of Ni at circum-neutral and basic pH. Depending on the availability of Al, both Ni-Al LDH and α-$Ni(OH)_2$ may act as important sinks for Ni. In soils and sediments composed of heterogeneous mixtures of mineral surfaces, it is forseeable that all three reactions, adsorption onto permanent or variable charge sites, precipitation of Ni-Al LDH and precipitation of α-Ni hydroxide may be active simultaneously.

4. CONCLUSIONS

The position of the $^3A_{2g}(^3F) \rightarrow {}^3T_{1g}(^3F)$ electronic transition ($\nu 2$) showed that α-$Ni(OH)_2$ formed in the presence of talc and amorphous silica, and Ni-Al LDH formed in the presence of pyrophyllite and gibbsite. The Al-for-Ni substitution in the hydroxide layers caused a band shift from 14,900 to 15,300 cm^{-1}. The Al substitution of the LDH precipitates may vary between 0.20 to 0.43 mole fraction. Variation of the Al substitution within that range did not significantly influence the position of $\nu 2$. Therefore, the small increase of $\nu 2$ over time may be explained by the growth of precipitate clusters. By providing an unequivocal discrimination of Al-containing versus Al-free hydroxide layers, DRS made an important contribution to the structural analysis of Ni surface precipitates. For kinetic Ni sorption experiments, Ni precipitates were detected by DRS at earlier stages than previously shown by XAFS. Although the formation of crystalline Ni phyllosilicates could be excluded based on the observed $\nu 2$ positions, the formation of Ni or Ni–Al phyllosilicate precursors may remain undetected by DRS. Thus, other methods are necessary to clarify this point.

Acknowledgments—We thank Brian McCandless for providing unlimited access to the UV-VIS-NIR spectrometer at the Institute for Energy Conversion, University of Delaware, and Richard Morris, NASA Houston, for providing the garnierite. Reviews by Gordon Brown Jr., Stanford University, Andre Scheidegger, Paul Scherrer Institut, Switzerland, and two anonymous reviewers greatly improved the quality of the manuscript. This work was funded by DuPont and the USDA.

REFERENCES

Abu-Eid R. M. and Burns R. G. (1976) The effect of pressure on the degree of covalency of the cation-oxygen bond in minerals. *Am. Mineral.* **61,** 391–397.

Bellotto M., Rebours B., Clause O., and Lynch J. (1996) A reexamination of hydrotalcite crystal chemistry. *J. Phys. Chem.* **100,** 8527–8534.

Bode H., Dehmelt K., and Witte J. (1966) Zur Kenntnis der Nickelhydroxidelektrode-I. Über das Nickel (II)-Hydroxidhydrat. *Electrochim. Acta* **11,** 1079–1087.

Brown G. E. Jr., Calas G., Waychunas G. A., and Petiau J. (1988) X-ray absorption spectroscopy and its applications in mineralogy and geochemistry. In *Spectroscopic Methods in Mineralogy and Geology* (ed. F. C. Hawthorne), Vol. 18, pp. 431–512. Mineralogical Society of America.

Burattin P., Louis C., and Che M. (1995) Étude des méchanismes physicochimiques mis en jeu au cours de la préparation par déposition-précipitation des catalyseurs Ni/SiO_2. *J. Chim. Phys.* **92,** 1377–1393.

Burattin P., Che M., and Louis C. (1997) Characterization of the Ni(II) phase formed on silica upon deposition–precipitation. *J. Phys. Chem. B* **101,** 7060–7074.

Burattin P., Che M., and Louis C. (1998) Molecular approach to the mechanism of deposition–precipitation of the Ni(II) phase on silica. *J. Phys. Chem. B* **102,** 2722–2732.

Burns R. G. (1993) *Mineralogical Applications of Crystal Field Theory*. Cambridge University Press.

Charlet L. and Manceau A. (1994) Evidence for the neoformation of clays upon sorption of Co(II) and Ni(II) on silicates. *Geochim. Cosmochim. Acta* **58,** 2577–2582.

Chisholm-Brause C. J., Brown G. E. Jr., and Parks G. A. (1989) EXAFS investigation of aqueous Co(II) adsorbed on oxide surfaces in-situ. *Physica B+C* **158,** 646–648.

Davidson A., Tempere J. F., Che M., Roulet H., and Dufour G. (1996) Spectroscopic studies of nickel(II) and nickel(III) species generated upon thermal treatments of nickel/ceria-supported materials. *J. Phys. Chem.* **100,** 4919–4929.

Depège C., El Metoui F.-Z., Forano C., de Roy A., Dupuis J., and Besse J.-P. (1996) Polymerization of silicates in layered double hydroxides. *Chem. Mater.* **8,** 952–960.

d'Espinose de la Caillerie J. B., Kermarec M., and Clause O. (1995) Impregnation of γ-alumina with Ni(II) and Co(II) ions at neutral pH: Hydrotalcite-type coprecipitate formation and characterization. *J. Amer. Chem. Soc.* **117,** 11471–11481.

Elzinga E. J. and Sparks D. L. (1999) Nickel sorption mechanism in a pyrophyllite-montmorillonite mixture. *J. Colloid Interface Sci.* **213,** 506–512.

Faye G. H. (1974) Optical absorption spectrum of Ni^{2+} in garnierite: A discussion. *Can. Mineral.* **12,** 389–393.

Ford R. G., Scheinost A. C., Scheckel K., and Sparks D. L. (1999) The link between clay mineral weathering and structural transformation in Ni surface precipitates. *Environ. Sci. Technol.* (in press).

Génin P., Delahaye-Vidal A., Portemer F., Tekaia-Elhsissen K., and Figlarz M. (1991) Preparation and characterization of α-type nickel hydroxides obtained by chemical precipitation: Study of the anionic species. *Eur. J. Solid State Inorg. Chem.* **28,** 505–518.

Grauby O., Petit S., Decarreau A., and Baronnet A. (1993) The beidellite–saponite series: An experimental approach. *Eur. J. Mineral.* **5,** 623–635.

Greaves C. and Thomas M. A. (1986) Refinement of the structure of deuterated nickel hydroxide, $Ni(OD)_2$, by powder neutron diffraction and evidence for the structural disorder in samples with high surface area. *Acta Crystallogr.* **B42,** 51–55.

Hemingway B. S. and Sposito G. (1996) Inorganic aluminum-bearing solid phases. In *The Environmental Chemistry of Aluminum* (ed. G. Sposito), pp. 81–116. Lewis Publisher.

Kamath P. V. and Therese G. H. A. (1997) On the existence of hydrotalcite-like phases in the absence of trivalent cations. *J. Solid State Chem.* **128,** 38–41.

Kermarec M., Decarreau A., Che M., and Carriat J. Y. (1995) Identification of supported phases produced in the preparation of silica-supported Ni catalysts by competitive cationic exchange. In *Preparation of Catalysts VI—Scientific Bases for the Preparation of Heterogeneous Catalysts* (ed. G. Poncelet), Vol. 91, pp. 967–976. Elsevier Science.

Krasovska O. V., Winkler B., Krasovskii E. E., Yaresko A. N., Antonov V. N., and Langer N. (1997) Ab initio calculation of the pleochroism of fayalite. *Am. Mineral.* **82,** 672–676.

Kubelka P. and Munk F. (1931) Ein Beitrag zur Optik der Farbanstriche. *Z. Tech. Phys.* **11,** 593–603.

Lever A. B. P. (1984) *Inorganic Electronic Spectroscopy.* Elsevier.

Liehr A. D. and Ballhausen C. J. (1959) Complete theory of Ni(II) and V(III) in cubic crystalline fields. *Ann. Phys.* **2,** 134–155.

Lindsay W. L. (1979) *Chemical Equilibria in Soils.* John Wiley & Sons.

Manceau A. (1990) Distribution of cations among the octahedra of phyllosilicates: Insight from EXAFS. *Can. Mineral.* **28,** 321–328.

Manceau A. and Decarreau A. (1988) Extended X-ray absorption fine-structure study of cobalt-exchanged sepiolite: Comment on a paper by Y. Fukushima and T. Okamoto. *Clays Clay Miner.* **36,** 382–383.

Manceau A., Calas G., and Decarreau A. (1985) Nickel-bearing clay minerals: I. Optical spectroscopic study of nickel crystal chemistry. *Clay Miner.* **20,** 367–387.

Marco de Lucas M. C., Rodríguez F., Prieto C., Verdaguer M., and Güdel H. U. (1995) Local structure determination of Mn^{2+} in the $ABCl_3$:Mn^{2+} chloroperovskites by EXAFS and by optical spectroscopy. *J. Phys. Chem. Solids* **56,** 995–1001.

Mattigod S. V., Rai D., Felmy A. R., and Rao L. (1997) Solubility and solubility product of crystalline $Ni(OH)_2$. *J. Solution Chem.* **26,** 391–403.

Mellini C. (1982) The crystal structure of lizardite 1*T*: Hydrogen bonds and polytypism. *Am. Mineral.* **67,** 587–598.

O'Day P. A., Brown G. E., and Parks G. A. (1994a) X-ray absorption spectroscopy of cobalt(II) multinuclear surface complexes and surface precipitates on kaolinite. *J. Colloid Interface Sci.* **165,** 269–289.

O'Day P. A., Rehr J. J., Zabinsky S. I., and Brown G. E. Jr. (1994b) Extended X-ray absorption fine structure (EXAFS) analysis of disorder and multiple-scattering in complex crystalline solids. *J. Amer. Chem. Soc.* **116,** 2938–2949.

O'Day P. A., Chisholm-Brause C. J., Towle S. N., Parks G. A., and

Brown G. E. Jr. (1996) X-ray absorption spectroscopy of Co(II) sorption complexes on quartz (α-SiO_2) and rutile (TiO_2). *Geochim. Cosmochim. Acta* **60,** 2515–2532.

Orgel L. E. (1952) The effects of crystal fields on the properties of transition metal ions. *J. Chem. Soc.* 4756–4761.

Orgel L. E. (1957) Ion compression and the colour of ruby. *Nature* **179,** 1348.

Pandya K. I., O'Grady W. E., Corrigan D. A., McBreen J., and Hoffman R. W. (1990) Extended x-ray absorption fine structure investigation of nickel hydroxides. *J. Phys. Chem.* **94,** 21–26.

Perdikatsis B. and Burzlaff H. (1981) Strukturverfeinerung am Talk $Mg_3[(OH)_2Si_4O_{10}]$. *Z. Kristallogr.* **156,** 177–186.

Pertlik F. (1985) Structures of hydrothermally synthesized cobalt(II) carbonate and nickel(II) carbonate. *Acta Crystallogr.* **C42,** 4–5.

Reinen D. (1966) Der Einfluss der kationischen Umgebung auf die Lichtabsorption des zweiwertigen Nickels in oxidischen Wirtgittern. *Theor. Chim. Acta* **5,** 312–326.

Reinen D. (1969) Ligand-field spectroscopy and chemical bonding in Cr^{3+}-containing solids. In *Structure and Bonding 6* (ed. P. Hemmerich et al.) Vol. 6, pp. 30–51. Springer-Verlag.

Scheidegger A. M. and Sparks D. L. (1996) Kinetics of the formation and the dissolution of nickel surface precipitates on pyrophyllite. *Chem. Geol.* **132,** 157–164.

Scheidegger A. M., Fendorf M., and Sparks D. L. (1996a) Mechanisms of nickel sorption on pyrophyllite: Macroscopic and microscopic approaches. *Soil Sci. Soc. Am. J.* **60,** 1763–1772.

Scheidegger A. M., Lamble G. M., and Sparks D. L. (1996b) Investigation of Ni sorption on pyrophyllite: An XAFS study. *Environ. Sci. Technol.* **30,** 548–554.

Scheidegger A. M., Lamble G. M., and Sparks D. L. (1997) Spectroscopic evidence for the formation of mixed-cation hydroxide phases upon metal sorption on clays and aluminum oxides. *J. Colloid Interface Sci.* **186,** 118–128.

Scheidegger A. M., Strawn D. G., Lamble G. M., and Sparks D. L. (1998) The kinetics of mixed Ni–Al hydroxide formation on clays and aluminum oxides: A time-resolved XAFS study. *Geochim. Cosmochim. Acta* **62,** 2233–2245.

Scheinost A. C., Schulze D. G., and Schwertmann U. (1999) Diffuse reflectance spectra of Al substituted goethite: A ligand field approach. *Clays Clay Miner.* **47,** 156–164.

Schoonheydt R. A., Roodhooft D., and Leeman H. (1987) Coordination of Ni^{2+} to lattice oxygens of the zeolites X and Y. *Zeolites* **7,** 412–417.

Schutz A. and Biloen P. (1987) Interlamellar chemistry of hydrotalcites I. Polymerization of silicate anions. *J. Solid State Chem.* **68,** 360–368.

Shannon R. D. (1976) Revised effective ionic radii and systematic studies of interatomic distances in halides and chalcogenides. *Acta Crystallogr. A* **32,** 751–767.

Taylor R. M. (1984) The rapid formation of crystalline double hydroxy salts and other compounds by controlled hydrolysis. *Clay Miner.* **19,** 591–603.

Towle S. N., Bargar J. R., Brown G. E., and Parks G. A. (1997) Surface precipitation of Co(II)(aq) on Al_2O_3. *J. Colloid Interface Sci.* **187,** 62–82.

Verberckmoes A. A., Weckhuysen B. M., Pelgrims J., and Schoonheydt R. A. (1995) Diffuse reflectance spectroscopy of dehydrated cobalt-exchanged faujasite-type zeolites: A new method for Co^{2+} siting. *J. Phys. Chem.* **99,** 15222–15228.

Weckhuysen B. M., Spooren H. J., and Schoonheydt R. A. (1994) A quantitative diffuse reflectance spectroscopy study of chromium-containing zeolites. *Zeolites* **14,** 450–457.

Zabinsky S. I., Rehr J. J., Ankudinov A., Albers R. C., and Eller M. J. (1995) Multiple scattering calculations of X-ray absorption spectra. *Phys. Rev. B* **52,** 2995.